Identification and compensation of error sources in the microbond test utilising a reliable high-throughput device

Composites Part A 137 (2020) 105988

Contents lists available at ScienceDirect

Composites Part A

journal homepage: www.elsevier.com/locate/compositesa

Identification and compensation of error sources in the microbond test utilising a reliable high-throughput device

P. Laurikainen[a,*], M. Kakkonen[b,**], M. von Essen[b], O. Tanhuanpää[b], P. Kallio[c], E. Sarlin[a]

[a] Tampere University, Faculty of Engineering and Natural Sciences, PO Box 589, FI-33014 Tampere University, Finland
[b] Fibrobotics Oy, Finland
[c] Tampere University, Faculty of Medicine and Health Technology, PO Box 692, FI-33014 Tampere University, Finland

ARTICLE INFO

Keywords:
Microbond test
Polymer-matrix composites (PMCs)
Interface/interphase
Fibre/matrix bond

ABSTRACT

This paper addresses the issue of high scatter in microbond test results. Implementation of the test is discussed and the reliability of a state-of-the-art test system is analysed through characterisation of the critical components of the device. In total 50 filaments and around 30 droplets from each filament are measured. The results verify that much of the commonly observed scattering originates from real variation between the filaments and heterogeneous interfacial properties, while the error from the experimentation is comparably small. A stress based analytical model was noted to agree well with the experimental results.

1. Introduction

Fibre reinforced composites are known as some of the best materials for high performance applications that require excellent strength-weight characteristics. To achieve adequate properties on the product level, the interfacial properties of the fibre-resin system must be optimised. This entails proper wetting of the fibres and adequate stress transfer between the fibres and the resin, both of which are mostly controlled by the sizing applied on the fibre surface [1,2]. Development of the sizing and fibre-resin systems in general requires testing the resulting interfacial properties. A common measure for the stress transfer capabilities of the interface is the interfacial shear strength (IFSS). The IFSS is measured with single fibre methods, such as the microbond test [3] and the single fibre pull-out test [4]. However, results tend to vary significantly between different testing methods and different studies [5]. This study aims to provide further insight to the causes of the variation and to explore methods for minimizing the role of implementation related error in the total scatter.

In the microbond test, single fibre microcomposite samples are tested in a modified scheme of the pull-out method. Resin droplets are deposited and cured on single filaments and after curing loaded with microvise blades until the droplet detaches from the fibre surface. The load required for the debonding is compared with the surface area of the fibre covered by the droplet to calculate the apparent IFSS. An overview of the microbond test is presented in Fig. 1.

Several possible error sources have been identified in the microbond test. The review by Sockalingam and Nilakantan [6] lists many of the error sources discussed in literature, from limitations in the experimental setup, behaviour of the materials both during sample preparation and testing to the limitations of the data analysis methods. In the device, critical aspects to minimise the scatter include high sampling rate of load measurement, accurate determination of fibre and droplet dimensions in addition to microvise blade control [7]. The microvise blade placement is one of the most important of these error sources because it is considered a major contributor to the high scatter of results [8–11]. The sample preparation should be as reproducible as possible and ensure a reasonable range of embedded lengths, for example, to avoid fibre breakage [6]. The curing of thermoset resins or the crystallisation of thermoplastic materials must be controlled to reduce variation of the results [12,13]. Miller et al. [3,7] have also pointed out an important source of variation that is commonly overlooked: the variation of the fibre surface itself. This variation, especially between filaments, has been noted in our previous work [14] and is based on tests where multiple droplets are deposited on a single filament close to each other. This possibility was discussed in the study presenting the microbond test by Miller et al. [3], but has not been validated due to limitations in the implementation. An overview of the current understanding of microbond error sources is collected in Table 1.

Reproducible and accurate control of the microvise is crucial to control the stress distribution during the microbond test and to avoid,

* Corresponding author.
** Corresponding author.
E-mail addresses: pekka.laurikainen@tuni.fi (P. Laurikainen), markus@fibrobotics.com (M. Kakkonen).

https://doi.org/10.1016/j.compositesa.2020.105988
Received 27 April 2020; Received in revised form 27 May 2020; Accepted 31 May 2020
Available online 11 June 2020

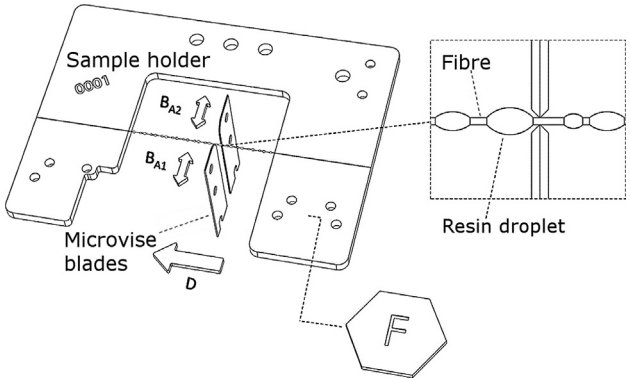

Fig. 1. An overview of the microbond test.

Table 1
Common error sources in microbond testing.

Error source	Possible negative outcomes	Ref.
Load measurement	Over-/underestimation of the measured load	[7]
Device optics	Inaccurate embedded length and/or fibre diameter	[6,7]
Microvise control	Variation of droplet loading state, high scatter in final results	[8,9,11]
Embedded area range	Changes in test behaviour, fibre breakage	[15,16,6]
Fibre surface	Variation of the results, always present	[3,7]
Resin curing	Inconsistent results, increased scatter, resin failure	[12,13]

for example, overestimating the IFSS because of compressive loads [8]. Chou et al. [8], Heilhecker et al. [9] and Nishikawa et al. [11] have explored the role of the microvise placement experimentally. Chou et al. [8] proposed an analysis to divide the force into shearing and compressive components to alleviate the issue. They also made a general observation that the gap width should be kept as small as possible. Heilhecker et al. [9] presented results from similar tests and complemented the results with finite element analysis (FEA). The FEA revealed significant difference between the maximum shear stress theory of failure and IFSS calculated from a maximum load during the test. However, no significant conclusions could be drawn due to very high scatter of the experimental results. Nishikawa et al. [11] stated that in order to analyse the true interfacial properties from microbond tests, one has to use FEA to determine the overall damage process in the test. Their FEA analysis of the microvise placement concludes that to avoid matrix cracking one should place the microvise blades as far apart as possible. However, their analysis did not include consideration for the possible increased compressive component presented by Chou et al. [8] or the tensile dominated mode of initial crack formation at the droplet meniscus [17,18]. Ash et al. [10] used FEA to observe the role of blade contact point and the stiffness of the interphase to the results of the microbond test and noted the importance of the microvise blade placement in relation to the droplet shape. Their model also predicted significant tensile stress components at the interface and an increase in debonding load, if the vise angle is increased as reported earlier by Chou et al. [8]. Given the attention it has received as an error source in microbond testing, accurate and reproducible control of the microvise placement is crucial in producing reliable microbond test data.

No standardised methodology exists for microbond testing, which has led to different research groups utilising very different equipment for the test. A common approach, also utilized by Miller et al. [3] in the study presenting the method, is to use universal testing systems with small load cells [3,19,20,12]. Reliable measurement of microscopic properties requires, however, equipment designed for the appropriate scale [6,7].

In this study, we aim to estimate the importance of the various error sources often regarded as major limitations in the utilisation of the microbond method and to seek ways to mitigate their role in the testing. By controlled deposition and measurement of 30 to 50 droplets of variable sizes on 50 single filaments we demonstrate the variation in the properties of sized glass fibre surfaces. This will include demonstrating the importance of measuring large number of individual droplets, possible only with a high throughput device, to ensure that the measured data reliably presents the natural variation of the IFSS. We will also compare our data to an existing analytical model to further understand the behaviour of the material during the test.

2. Experimental

2.1. Device overview

The main sources of device related errors in microbond measurements are the load measurement, determination of embedded length, displacement actuator movement and the placement of the microvise blades. The FIBRObond device (Figure S1), presented here, is designed to reduce the impact of these error sources.

In the device, load is measured with a Futek (US) jr. S-beam 1 N cell. The cell is connected to a linear slide, which is connected to an absolute linear encoder manufactured by Numerik Jena (Germany). The load measurement method differs from the typical setup presented in microdroplet test publications. The main differences are the horizontal loading direction and the linear slide, connecting the sample to the load cell, intended to reduce load components that are not aligned to the horizontal axis direction. The encoder connected to the slide is used for determining elastic deformation of the load cell during loading. The components of the load measurement are presented in Fig. 2. National instruments (US) NI-6003 data acquisition (DAQ) device is used to record the signal with a 1 kHz frequency. During the measurement, the droplet is displaced using R35 microtome blades manufactured by Feather (Japan). Both blades can be moved separately to adjust the blade placement and the blade gap using piezo actuators manufactured by SmarAct (Germany). The fine resolution (5 nm) of the actuators, with the accurate imaging through the device optics enables placing the blades in contact with fibre without damaging the fibre itself. This enables reproducible control of the blade gap. Alignment of the blades is controlled using shimmers and can be monitored via the device optics. During the assembly, the alignment of the blade centre lines is controlled with 2 μm tolerance and checked regularly. This is crucial to minimize error caused by blades in the measurements as even very small misalignment causes bending of the fibre and uneven loading of the droplet during a test. The movement along the fibre is controlled with a M-111.1DG1 DC motor (see Fig. 3) operated with a C-863 controller manufactured by Physik Instrumente (Germany). During the testing the, speed is 0.008 mm/s.

The optics of the device comprise a tube microscope with a 20x long working distance objective and a 2x extender tube manufactured by Qioptiq (United Kingdom). The view is captured with an IDS (Germany) UI-3370SE monochromatic camera. The field of view was calibrated using a microscope micrometer manufactured by Helmut Hund (Germany) with a 1 mm measuring line with 100 divisions. Scale factor for this optic setup is 0.137 μm/px (280.576 μm × 280.576 μm field of view).

To analyse the embedded length of a droplet from the captured view, a computer vision algorithm was developed. Snapshots of the algorithm steps are presented in Figure S2. The algorithm utilises threshold conversion of the image to binary, filling of enclosed white contours and cropping black pixels from pixel columns that have less black pixels than a pre-set threshold defined by a user. A smallest confining rectangle is fitted over each droplet and the length of the box is measured. This automated, algorithm-based method is hypothesized to give more consistent measurements than human operation.

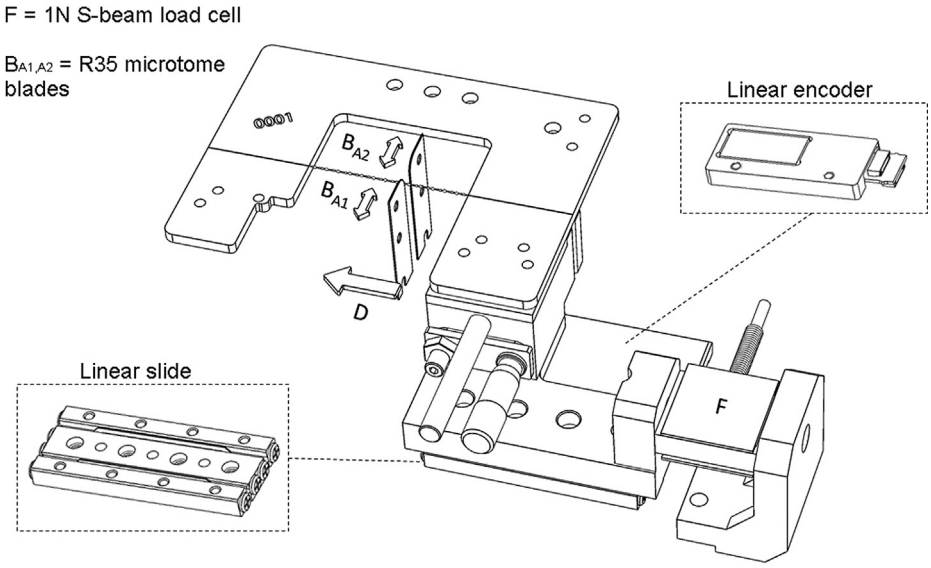

Fig. 2. The critical components of the load measurement implementation in the device.

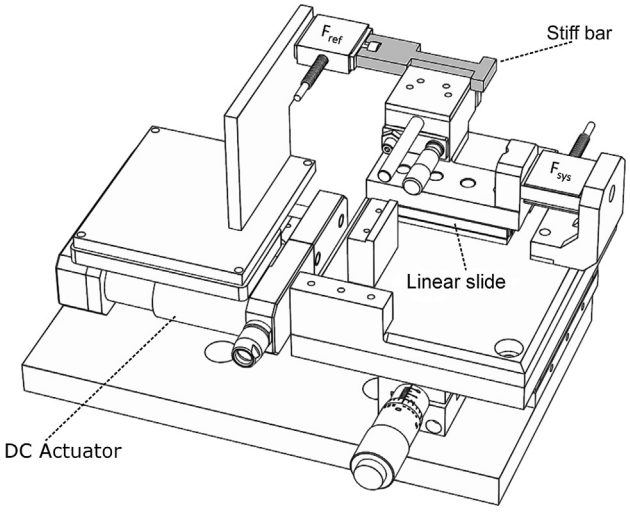

Fig. 3. Setup for calibrating the force measurement.

2.2. Validation of the system

The performance of the critical components of the device – the load measurement, total displacement and the device optics – were tested to analyse the total error from the measurement system and validate the accuracy of the device in microscale testing. The load cell calibration provided by the manufacturer was validated using free weights. In order to calibrate the force measurement in the system, a special setup for the calibration was developed. The calibration setup comprises the system load cell (F_{sys}) connected to a reference cell (F_{ref}) via a stiff bar shown in Fig. 3. The reference cell is the same model and from the same manufacturer as the system load cell. Calibration was conducted with five force levels, repeating five times for each loading level. The average of these five measurements was calculated for both force cells and the ratio between the averages were used to determine a calibration factor for the force. The total displacement during a test results from the actuator movement and the elastic deformations of the load cell, the sample holder and the filament. The procedure and outcomes of the determination of displacement accuracy are included in the supplementary data.

Accuracy of the computer vision algorithm compared to human operators was studied with a group of five operators. This group contained both researchers familiar with microbond testing and researchers outside of the field. The operators measured dimensions of a predetermined series of droplets with a high-end optical microscope and with the vision system of the FIBRObond device. The images from the FIBRObond device were analysed both manually, using image analysis software and with the computer vision algorithm. Parameters of the microscope and illumination were kept constant for all operators. The affecting factors should therefore be the operator, their opinion on how the droplet size should be determined and the capabilities of the method itself.

2.3. Materials

An average of 40 droplets were deposited over a length span of 10–12 mm on a 15 cm long filament. These filaments were selected from a roving of HiPer-tex W 2020 glass fibre, kindly provided by Ahlstrom-Munksjö Glassfibre Oy. The filaments were taken in batches of 10 from controlled length regions of the roving, approximately 150 mm apart. The fibres were measured within the intended storage lifetime, to ensure the viability of the sizing on the fibres. Table 2 shows the properties of the W 2020 fibre along with the average diameter of the filaments used in this study.

Araldite LY 5052 epoxy resin was used for the droplets. The resin was selected due to its high stiffness and predictable curing allowing us to reduce the role of resin variation in the results. The time window for droplet deposition was selected from 15 min to 45 min after mixing. The selection was based on the pot life given in the resin datasheet and

Table 2
Material properties.

Material	E_A/E_m [GPa]	CTE (α) [$\times 10^{-6}$ 1/K]	Fibre ∅ [μm]	Poisson's ratio
HiPer-tex W 2020 [21]	86	4.1	18.6 ± 1.3	0.17 [22]
Araldite LY 5052 [23]	3.35	71.0	–	0.35

observations made during the sample preparation. In the selected timeframe, the behaviour of the resin batch did not change noticeably. The cure cycle for the deposited droplets was also selected based on the datasheet: one day at room temperature followed by eight hours at 80 °C. Bulk resin, cured with this cure cycle would have a glass transition temperature around 120 °C. The cure cycle is therefore assumed to result in a reasonably high degree of cure even for a microscale resin batch. The resin properties needed for analysis are also collected to Table 2.

A total of 50 filaments were measured, adding up to approximately 1500 individual droplet measurements. The large dataset enables a thorough analysis of the variation of the fibre surface and other possible sources of deviation. It also demonstrates the high-throughput capabilities of the equipment in use. The droplets were prepared with embedded lengths ranging approximately from 50 to 180 μm to observe the embedded area dependency of the debonding load.

3. Results

3.1. Device validation

The operation of the load cell was validated both as standalone and in the system to ensure the accuracy of the load measurement during the microbond tests. Outside of the system the voltage to load conversion of the cell follows the coefficient of 0.09815 N/V. In the measurement system, the force cell also measures some minor frictional components causing a slight difference between the loads F_{ref} and F_{sys} in the calibration setup. The coefficient is therefore slightly lower, 0.09758 N/V. The results of the calibration measurements are presented in Fig. 4. The in-system coefficient was used for voltage-load conversion and the standard error of regression for the coefficient was included into the error analysis. As the load cell operates with a high sampling rate and very low forces, it is unsurprising that the load measurement has notable noise in the data. During the analysis, this noise was filtered with a 50 point moving average, which was enough to remove the noise almost completely. However, this also causes some level of uncertainty to the measured debonding load. This uncertainty is, however, several orders of magnitude smaller than the error of the voltage to load conversion and deemed negligible to the total error.

The accuracy and reproducibility of the embedded length measurement are critical factors in microbond testing. The three methods explained in Section 2.2 for determining the embedded lengths were compared for five operators. The standard deviations (σ) were calculated for each droplet based on the results from each operator. The standard error ($\sigma_{\bar{x}}$) of each method is estimated from the average standard deviation for the method and the number of analysed droplets. An overview of the results is provided in Table 3. Overall, the accuracies of the three methods are similar and the variation between operators small. However, for extremely small droplets, e.g. 30–40 μm or with occasional errors in manual operation, the variation can be significantly higher than the average. The largest contributor to the deviation was the operators' interpretation of the two ends of the droplet.

Table 3
Statistical comparison of the embedded lengths measured by 5 operators with 3 different methods.

Method	# of droplets	max. σ [μm]	min. σ [μm]	ave. σ [μm]	$\sigma_{\bar{x}}$ [μm]
Computer vision	64	5.38	0.85	1.75	0.219
Image analysis	76	4.11	0.85	1.84	0.211
Microscope	77	5.37	0.53	2.16	0.246

3.2. Microbond measurements

The IFSS of the HiPer-tex W 2020 glass fibre – Araldite LY 5052 microcomposites was determined by measuring the load required to debond a total of 1527 microdroplets with varying embedded lengths. This sampling represents the glass fibre roving from a length of approximately 1.3 m. Droplets deposited into close proximity of each other on the same filaments exhibit very similar interfacial properties. The strain rate in each test is also similar and has no significant effect on the results. Together these factors – coupled with accurate control of the microvise blade gap to the fibre surface – enable the measurement of data with very low scatter within a single data series. Results for filaments numbered # 4, # 22 and # 37 are presented Fig. 5 as examples. These results were selected to show the quality of the data and represent their respective roving spans (i.e. 0 to 15 cm for filament # 4). As can be observed from Fig. 5, the results for droplets deposited on a single filament exhibit a linear behaviour. Significantly more scatter emerges when the variation between different filaments is included. This is already seen in Fig. 5, but is even more clear when all the measured data is plotted together (see Fig. 7). Calculating the apparent IFSS for individual droplets of the full dataset results in IFSS of 31.71 ± 6.70 MPa. Using linear regression to determine the IFSS from the slope of the force vs. embedded area from the full dataset as done by Cai et al. [24], results in an average IFSS of 45.77 ± 0.50 MPa. Note that

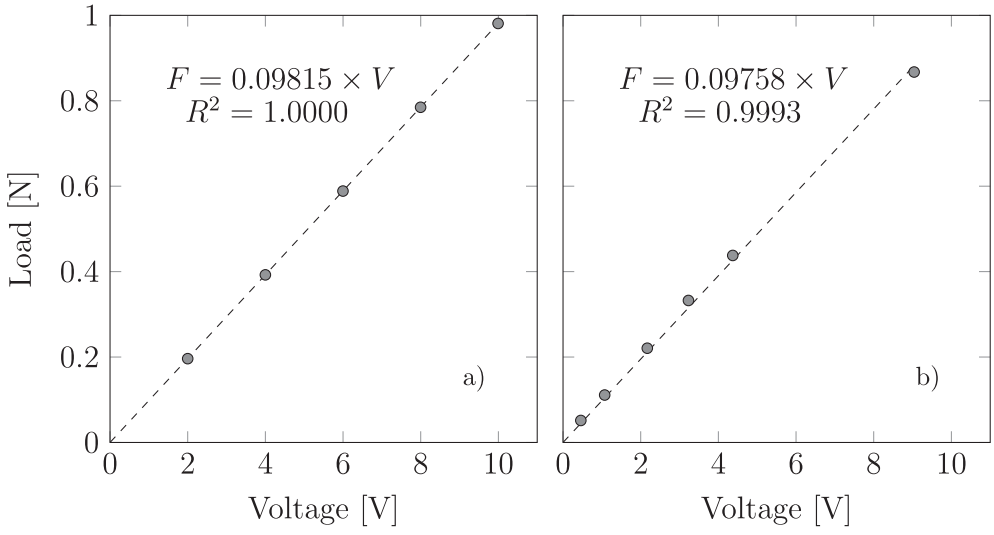

Fig. 4. Voltage to load conversion calibration, a) standalone, b) in system.

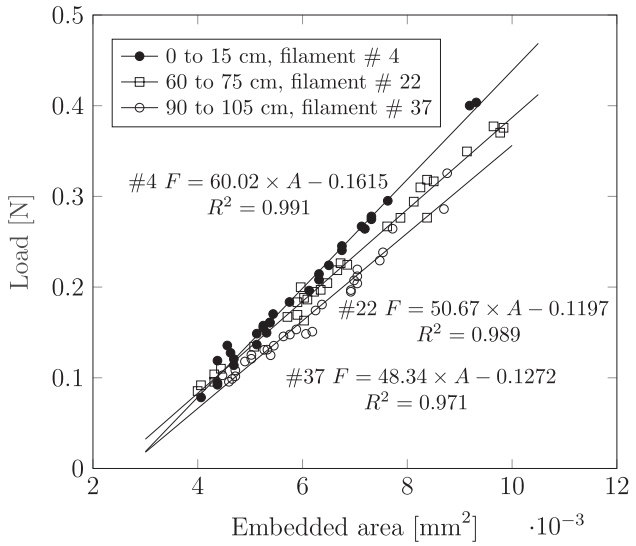

Fig. 5. Single filament data series examples from three different sections of roving.

in this case the error value ± 0.50 MPa is the standard error of the slope from the linear regression. Linear regression for the 50 filaments separately, taking the average slope as IFSS, results in 52.76 ± 9.79 MPa. The average IFSS also varies along the length of the roving. The average IFSS for 10 parallel samples from a single roving section varies between 57.32 ± 5.36 MPa and 49.72 ± 9.75 MPa. It is clear that the apparent IFSS, without further analysis, is not a suitable measure for the behaviour of the interface.

4. Discussion

Most methods of analysis for microbond results do not consider the role of displacement. However, to improve the applicability of the method from comparative studies, the incorporation of more in-depths analysis such as FEA is needed and the validation of FEA requires accurate force-displacement information from the test. Similarly to FEA, the displacement is an important parameter in analysis methods which consider the crack propagation, such as the analysis proposed by Lilholt and Sørensen [25]. Many aspects of the displacement error, such as the elastic deformation of the load cell (see Figure S3), can be fairly easily compensated or even ignored. The strain rate however, needs to be controlled and accurate for reliable testing and the performance of the movement actuator is crucial, as can be seen in Figure S4.

The error in the estimation of the embedded area can cause significant scattering of microbond results. Most importantly the estimation should be consistent. Consistent over- or under-evaluation of the embedded lengths can still result in a low scatter of the data. This however, shifts the data accordingly and makes the apparent IFSS from individual droplets very unreliable. The significance of operator and method variation on the results was examined by comparing the results of sample # 24, which was used in embedded area analysis by different operators. The variation of the computer vision results between the operators and the variation between the methods for a single, representative operator are presented in Fig. 6. The reproducibility of the computer vision is slightly better compared to the other methods. The computer vision and optical microscope result in very similar slopes, with some variation in the axis intercept, whereas the results from manual image analysis differed noticeably. For one operator however, the slopes were almost identical for all three methods and the results of computer vision and microscope were close to identical. The most important outcome of the analysis are the similar slopes from microscope and computer vision methods. Therefore, there is little difference in the slope-based IFSS analysis for the two methods.

The level of uncertainty in the microbond measurements was determined by calculating the sum of errors from all relevant error sources. The formulation is presented in the supplementary data. The error in IFSS from the experimentation was determined as 3.00 ± 0.70 MPa. The uncertainty of embedded length was identified as the most important contributor and the result can be improved significantly if the operators' influence can be further mitigated. Even with some uncertainty in the embedded area determination, the total error from experimentation is significantly lower than the natural variation of the IFSS, which for our results is in the range of 7 to 10 MPa.

Modern analysis of microbond results utilizes usually either FEA or analytical models to better understand the test system and the results in terms of actual material behaviour. The apparent IFSS (τ_{app}) is, as discussed in Section 3.2, a poor measure of the true interfacial performance as it fails to account for important factors such as thermal residual stresses. To better understand the results, the data is fitted to the stress based model presented by Zhandarov and Mäder [22]. The model includes the Nayfeh shear lag parameter β presented as

$$\beta^2 = \frac{2}{r_f^2 E_A E_m}\left[\frac{E_A V_f + E_m V_m}{\frac{V_m}{4G_A} + \frac{1}{2G_m}\left(\frac{1}{V_m} ln \frac{1}{V_f} - 1 - \frac{V_f}{2}\right)}\right] \quad (1)$$

where E_A, E_m, G_A and G_m are the tensile and shear modulus of the fibre and the matrix, respectively. V_f and V_m are the volume fractions of the two components and r_f is the fibre radius. To calculate the volume fractions, the resin droplets are approximated using an elliptical shape with a length equal to l_{emb} and a maximum thickness equal to the droplet maximum thickness.

The aforementioned formulation for the shear lag parameter resulted in negative β^2 values for some of the smallest droplets. This is a known feature of the Nayfeh parameter when the fibre volume fraction is higher than a certain material dependent critical value [22]. To still include these droplets into the analysis, the Cox shear lag parameter is used to analyse these droplets [16] despite its limitations [22] as it is generally well behaved for higher fibre volume fractions [16,22,26].

$$\beta^2 = \frac{2G_m}{E_A ln\left(\frac{1}{V_f}\right)} \quad (2)$$

The shear lag parameter can be used to estimate the thermal residual stresses τ_T with

$$\tau_T = \frac{\beta r_f E_A}{2}(\alpha_A - \alpha_m)\Delta T \quad (3)$$

where α_A and α_m are the fibre and resin thermal expansion coefficients (Table 2) and ΔT is the temperature difference from stress free temperature and testing conditions. In this case it is taken as the difference between the curing temperature (80°C) and approximate lab temperature of 23 °C.

Zhandarov and Mäder [22] present two cases of debonding event. The first case is a catastrophic crack propagation through the embedded length where the friction at the interface does not contribute to the measured load. The second is a stable crack propagation case where the interfacial friction needs to be considered a part of the loading case. These two analysis cases are determined by the conditions $\beta l_{emb} < ln(u + \sqrt{(u^2 + 1)})$ and $\beta l_{emb} \geqslant ln(u + \sqrt{(u^2 + 1)})$, where u is a parameter defined as

$$u = \frac{\sqrt{\tau_T^2 + 4\tau_f(\tau_d - \tau_f)} - \tau_T}{2\tau_f} \quad (4)$$

where τ_f and τ_d are the interfacial friction and interfacial shear strengths, respectively. We have evaluated the interfacial friction based on the embedded area and the load level after the debonding event [27]. In some measurements, however, no such load was detected after

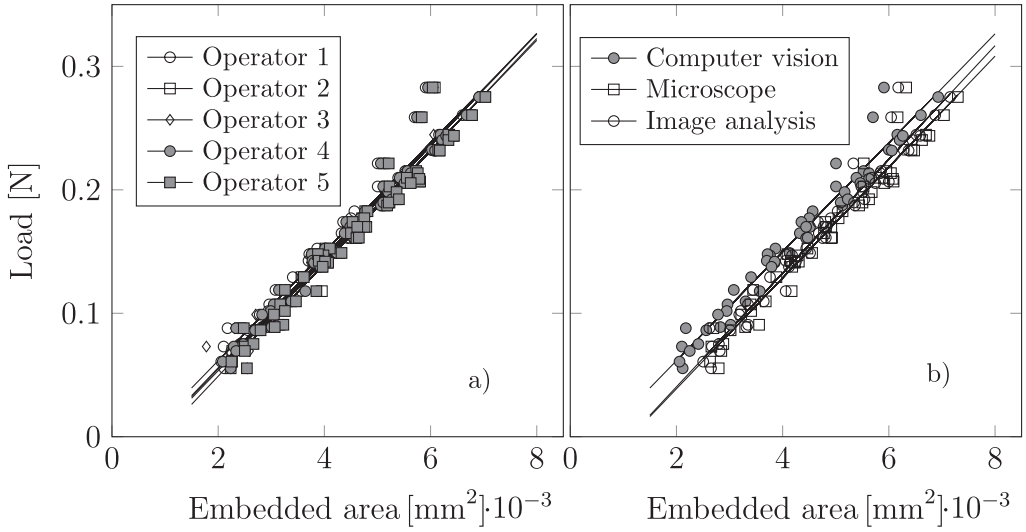

Fig. 6. Filament # 24 analysed with embedded areas measured with a) computer vision by all five operators, b) all three methods by operator 1.

Table 4
Distribution of the result to the three analysis cases defined in

Case	# of droplets	Explanation of the case
1: $\tau_f \approx 0$	277	No friction force detected
2: $\beta l_{emb} < ln(u + \sqrt{(u^2+1)})$	1146	Catastrophic debonding [22]
3: $\beta l_{emb} \geqslant ln(u + \sqrt{(u^2+1)})$	104	Stable crack propagation [22]

debonding and these have been included in the analysis as a separate third case. The result of the linear regression based analysis presented in Section 3.2 was used for each filament dataset as the interfacial shear stress τ_d. Table 4 presents the distribution of the results into these three analysis cases. The first two cases in Table 4 are analogous as the analytical formulations for the frictionless case and the catastrophic debonding case are the same. Only the third case takes the friction forces into account in the analysis. The model used to predict the maximum load for each droplet has the form [22]:

$$F_{max}(l_{emb}) = \begin{cases} \frac{2\pi r_f}{\beta}\left[\tau_d tanh(\beta l_{emb}) - \tau_T tanh(\beta l_{emb}) tanh\left(\frac{\beta l_{emb}}{2}\right)\right], & \text{for 1, 2} \\ \frac{2\pi r_f}{\beta}\left[\tau_d \frac{u}{\sqrt{(u^2+1)}} - \tau_T\left(1 - \frac{1}{\sqrt{(u^2+1)}}\right) + \tau_f\left[\beta l_{emb} - ln\left(u + \sqrt{(u^2+1)}\right)\right]\right], & \text{for 3} \end{cases} \quad (5)$$

The output from the model presented in Eq. (5) is the expected maximum force for a microbond measurement of that droplet. Fig. 7 presents the full measured dataset and the model predictions for comparison. As can be seen from the figure, the model predicts the experimental behaviour very well. The fit is poorer for the droplets analysed with the Cox shear lag parameter, visible as the series of higher loads at low embedded areas. The axis offset results mostly from the thermal stresses and is accurately predicted by the model.

Based on this analysis, the role of the interfacial friction is overall minor. Only a small percentage of the droplets fulfil the condition for stable crack propagation and, according to the model, require consideration for the friction component. In Fig. 8, the relative portion of the force associated with interfacial friction is plotted against the corresponding fibre volume fraction. The results indicate that even relatively large frictional forces can be measured without requiring consideration for them in the final analysis. However, the Cox shear lag parameter does not appear to function properly for this part of the analysis, as those droplets are grouped into case 2. At least some, if not all, would be expected to fulfil the case 3 condition based on Fig. 8. The role of interfacial friction in microbond testing requires further experimental study to be fully understood.

For further comparison, the model presented in Eq. (5) was fitted to the measured maximum load values to estimate the IFSS (τ_d). These results are presented in Fig. 9. Based on the results, we can detect a lower limit for the embedded length after which the experimental and analytical results coincide well. It should be noted that these smallest droplets are also quite unreliable to measure and were included more to test the limits of the device. Limiting the measured droplets to embedded lengths around 55 μm and above would significantly mitigate any issues. This lower limit depends on the fibre dimensions – and to a lesser extent on the fibre-resin combination [22] – and is therefore difficult to predict before measurement. An overview of the IFSS analysed with the methods presented in this paper is shown in Table 5. For the analytical model, limiting the analysis only to droplets above 55 μm in embedded length gives an average IFSS of 47.85 ± 7.83 MPa. The interfacial properties vary along the roving length, with the highest values measured from the start of the roving.

The validity of the maximum load based apparent IFSS as a measure for interfacial strength has been under much discussion, with some publications stating it as not valid, e.g. [15,28]. This is true if the analysis only considers the maximum load from a single measurement, but simply measuring a range and estimating the slope can give a good approximation of true interfacial properties without needing more complex methods of analysis. Many studies, utilise the more traditional pull-out scheme – where the sample behaviour during the test is vastly different – or microbond with large droplets in the range of 100–500 μm or even larger. Based on our experience, when measuring smaller droplets (e.g. from 50–200 μm as in this paper) the test usually follows the optimal behaviour of catastrophic debonding, as is also predicted by the stress based analytical model. The behaviour of the analytical model for other fibre-resin systems needs to be explored in future work. For many resin systems, the final properties of a microscale sample are much less predictable and finding suitable parameters for the model may prove more difficult. On the other hand, if the model performs equally well, fitting to the model could help predict the properties in cases where direct measurements are difficult or impossible.

The important outcome is that the average IFSS for the droplets on a single filament can be quickly evaluated from the slope seen in Fig. 5 with reasonable accuracy. The fibre-resin system is then characterised by measuring several filament samples. This approach enables simple

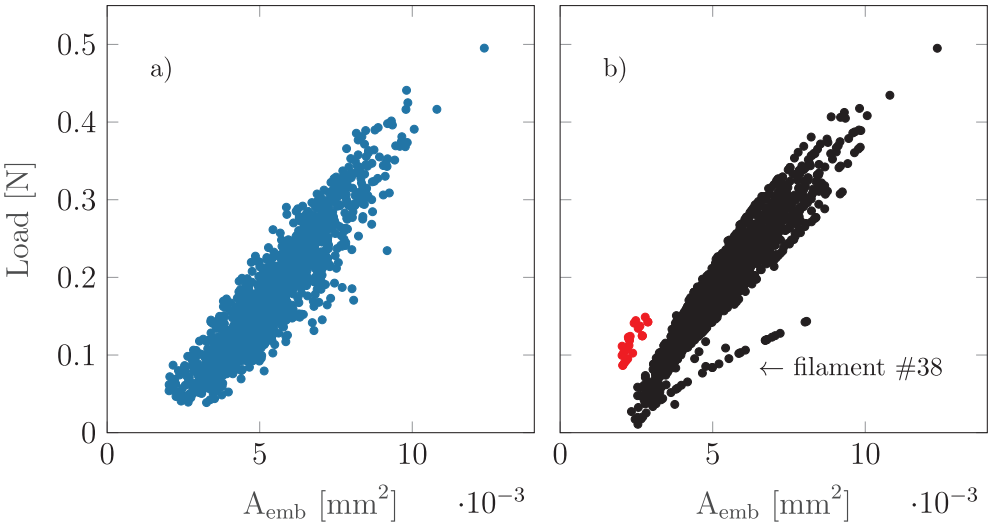

Fig. 7. Load vs. embedded area for all measured droplets, a) Measured data, b) Data based on the model. The weaker dataset from filament # 38 is clearly visible in the model data. Data points analysed with the Cox shear lag parameter are indicated in red. (For interpretation of the references to color in this figure legend, the reader is referred to the web version of this article.)

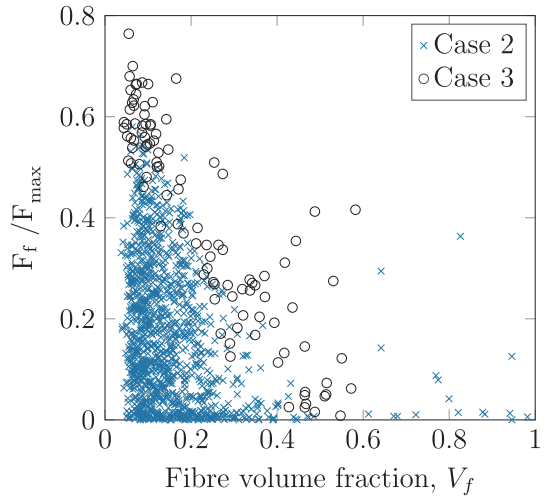

Fig. 8. Role of interfacial friction based on the stress based analysis, separated into cases according to Table 4. (For interpretation of the references to color in this figure legend, the reader is referred to the web version of this article.)

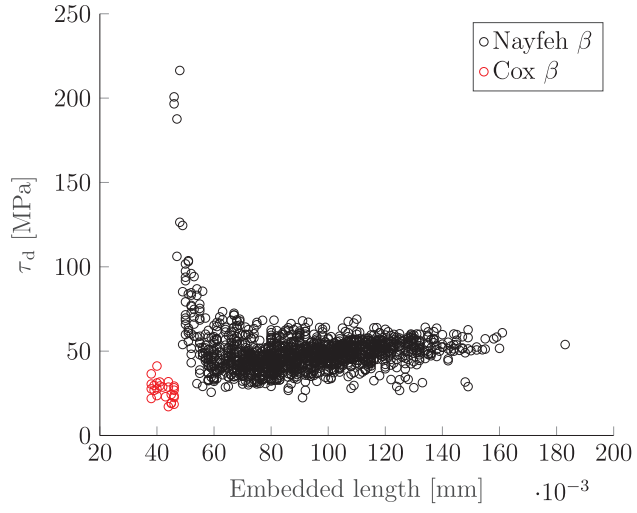

Fig. 9. IFSS (τ_d) analysed according to Eq. (5) vs. droplet embedded length. (For interpretation of the references to color in this figure legend, the reader is referred to the web version of this article.)

Table 5
Overview of the Araldite LY 5052 - HiPer-tex W 2020 IFSS with various analysis methods.

Roving section [cm]	Individual droplets, τ_{app}	Linear regression, all data [24]	Linear regression, filaments	Stress based model [22]
0–15	33.62 ± 6.48	–	57.32 ± 5.36	52.44 ± 13.63
30–45	31.87 ± 7.12	–	53.77 ± 5.00	48.84 ± 16.55
60–75	31.47 ± 5.63	–	51.95 ± 5.32	47.81 ± 11.41
90–105	30.95 ± 7.18	–	49.72 ± 9.75	47.74 ± 10.68
120–135	29.95 ± 6.60	–	50.01 ± 6.28	45.47 ± 10.62
Average	31.71 ± 6.70	45.78 ± 0.50	52.76 ± 9.79	48.68 ± 12.84

and reliable analysis of the interfacial properties and provides valuable input for a more thorough analysis of the micromechanics of the system.

The preparation of suitable samples can be challenging. One possible sample preparation scheme has been proposed by Hou and Sun [29], who presented a polymer solution based method for samples with multiple droplets on each filament. Sample preparation is also important in terms of the final droplet shape. Inconsistent sample behaviour can therefore be expected to increase the scatter of the experimental results and make the direct estimation of the IFSS from the experimental results difficult. However, the analytic model can take the shape of the droplet into account and fitting the data to the model could therefore lead to more reliable analysis. In this study, however, the sample preparation was very predictable and the droplet thickness corresponds similarly to the embedded length in all samples.

5. Conclusions

The high scatter of microbond results can be mitigated by minimizing the device related scatter and by measuring multiple droplets with a suitably wide range of droplet sizes from a single filament. The embedded length range should favour immediate debonding so that the maximum force corresponds linearly to the embedded area. However, measuring too small droplets can also hinder the analysis and the lower limit should be identified before, or early during, the measurement. Working on this scale requires accurate equipment and the sample preparation needs to have suitable control over the embedded length distribution. Based on our results, 30 droplets for each filament is sufficient to analyse the interfacial properties. A suitably large number of filaments should be measured if one expects to reliably characterise the properties of the fibre-resin combination. Our results show variation of

the interfacial properties both between the individual filaments of the roving and along the length of the roving, which should be considered when selecting the samples. Stress based analysis is found to agree well with the experimental results and can be used to evaluate for example the contribution of thermal stresses to the measured results. The role of the microvise blade gap can be largely ignored by measuring with the blades touching, but not compressing, the fibre. By measuring with this methodology we characterised the average IFSS of W2020 glass fibres with Araldite LY 5052 epoxy resin as 52.76 ± 6.85 MPa, but in small sections of the roving the IFSS can be significantly lower, in the range of 20–25 MPa.

CRediT authorship contribution statement

P. Laurikainen: Conceptualization, Formal analysis, Investigation, Data curation, Writing - original draft, Writing - review & editing, Visualization. **M. Kakkonen:** Conceptualization, Methodology, Software, Investigation, Resources, Writing - original draft, Writing - review & editing. **M. von Essen:** Methodology, Software, Writing - review & editing. **O. Tanhuanpää:** Conceptualization, Methodology, Resources, Writing - review & editing, Visualization. **P. Kallio:** Conceptualization, Resources, Writing - review & editing, Supervision. **E. Sarlin:** Conceptualization, Resources, Writing - review & editing, Supervision.

Declaration of Competing Interest

The authors declare that they have no known competing financial interests or personal relationships that could have appeared to influence the work reported in this paper.

Acknowledgements

The study was partly financially supported by the Tampere University Graduate School as well as the Academy of Finland project “From micro-scale data to macro-scale understanding for improved safety of composite materials” (314983).

Appendix A. Supplementary material

Supplementary data associated with this article can be found, in the online version, at https://doi.org/10.1016/j.compositesa.2020.105988.

References

[1] Dey M, Deitzel J, Gillespie J, Schweiger S. Influence of sizing formulations on glass/epoxy interphase properties. Compos Part A: Appl Sci Manuf 2014;63:59–67. https://doi.org/10.1016/j.compositesa.2014.04.006.
[2] Teklal F, Djebbar A, Allaoui S, Hivet G, Joliff Y, Kacimi B. A review of analytical models to describe pull-out behavior – fiber/matrix adhesion. Compos Struct 2018;201:791–815. https://doi.org/10.1016/j.compstruct.2018.06.091.
[3] Miller B, Muri P, Rebenfeld L. A microbond method for determination of the shear strength of a fiber/resin interface. Compos Sci Technol 1987;28:17–32. https://doi.org/10.1016/0266-3538(87)90059-5.
[4] Penn LS, Bowler ER. A new approach to surface energy characterization for adhesive performance prediction. Surf Interface Anal 1981;3:161–4. https://doi.org/10.1002/sia.740030405.
[5] Pitkethly M, Favre J, Gaur U, Jakubowski J, Mudrich S, Caldwell D, et al. A round-robin programme on interfacial test methods, Compos Sci Technol 1993;48:205–14. doi: 10.1016/0266-3538(93)90138-7, Special Issue Microphenomena in Advanced Composites.
[6] Sockalingam S, Nilakantan G. Fiber-Matrix Interface Characterization through the Microbond Test. Int J Aeronaut Space Sci 2012;13:282–95. https://doi.org/10.5139/IJASS.2012.13.3.282.
[7] Miller B, Gaur U, Hirt DE. Measurement and mechanical aspects of the microbond pull-out technique for obtaining fiber/resin interfacial shear strength. Compos Sci Technol 1991;42:207–19. https://doi.org/10.1016/0266-3538(91)90018-K special Issue Interfaces in Composites.
[8] Chou C, Gaur U, Miller B. The effect of microvise gap width on microbond pull-out test results. Compos Sci Technol 1994;51:111–6. https://doi.org/10.1016/0266-3538(94)90161-9.
[9] Heilhecker H, Cross W, Pentland R, Griswold C, Kellar JJ, Kjerengtroen L. The vice angle in the microbond test. J Mater Sci Lett 2000;19:2145–7. https://doi.org/10.1023/A:1026787012473.
[10] Ash J, Cross W, Svalstad D, Kellar J, Kjerengtroen L. Finite element evaluation of the microbond test: meniscus effect, interphase region, and vise angle. Compos Sci Technol 2003;63:641–51. https://doi.org/10.1016/S0266-3538(02)00256-7.
[11] Nishikawa M, Okabe T, Hemmi K, Takeda N. Micromechanical modeling of the microbond test to quantify the interfacial properties of fiber-reinforced composites. Int J Solids Struct 2008;45:4098–113. https://doi.org/10.1016/j.ijsolstr.2008.02.021.
[12] Biro DA, McLean P, Deslandes Y. Application of the microbond technique: Characterization of carbon fiber-epoxy interfaces. Polym Eng Sci 1991;31:1250–6. https://doi.org/10.1002/pen.760311704.
[13] Zinck P, Wagner H, Salmon L, Gerard J. Are microcomposites realistic models of the fibre/matrix interface? ii. physico-chemical approach. Polymer 2001;42:6641–50. https://doi.org/10.1016/S0032-3861(00)00871-5.
[14] von Essen M, Sarlin E, Tanhuanpää O, Kakkonen M, Laurikainen P, Hoikkanen M, et al. Automated high-throughput microbond tester for interfacial shear strength studies. In: Proceedings of the SAMPE Conference 2017 Stuttgart, SAMPE Europe; 2017.
[15] Zinck P, Wagner H, Salmon L, Gerard J. Are microcomposites realistic models of the fibre/matrix interface? i. micromechanical modelling. Polymer 2001;42:5401–13. https://doi.org/10.1016/S0032-3861(00)00870-3.
[16] Scheer RJ, Nairn JA. A comparison of several fracture mechanics methods for measuring interfacial toughness with microbond tests. J Adhesion 1995;53:45–68. https://doi.org/10.1080/00218469508014371.
[17] Piggott M. A new model for interface failure in fibre-reinforced polymers. Compos Sci Technol 1995;55:269–76. https://doi.org/10.1016/0266-3538(95)00103-4.
[18] Zhandarov S, Gorbatkina Y, Mäder E. Adhesional pressure as a criterion for interfacial failure in fibrous microcomposites and its determination using a microbond test. Compos Sci Technol 2006;66:2610–28. https://doi.org/10.1016/j.compscitech.2006.03.023.
[19] Craven J, Cripps R, Viney C. Evaluating the silk/epoxy interface by means of the microbond test. Compos Part A: Appl Sci Manuf 2000;31:653–60. https://doi.org/10.1016/S1359-835X(00)00042-7.
[20] Day R, Rodrigez J. Investigation of the micromechanics of the microbond test. Compos Sci Technol 1998;58:907–14. https://doi.org/10.1016/S0266-3538(97)00197-8.
[21] HiPer-tex™W 2020 Rovings datasheet, 3B-the fiberglass company; 2018.
[22] Zhandarov S, Mäder E. Peak force as function of the embedded length in pull-out and microbond tests: effect of specimen geometry. J Adhes Sci Technol 2005;19:817–55. https://doi.org/10.1163/1568561054929937.
[23] Araldite LY 5052 Resin/ Aradur 5052 Cold curing epoxy systems, Huntsman Advanced Materials Inc.; 2012.
[24] Cai G, Wada M, Ohsawa I, Kitaoka S, Takahashi J. Interfacial adhesion of recycled carbon fibers to polypropylene resin: Effect of superheated steam on the surface chemical state of carbon fiber. Composi Part A: Appli Sci Manuf 2019;120:33–40. https://doi.org/10.1016/j.compositesa.2019.02.020.
[25] Lilholt H, Sørensen BF. Interfaces between a fibre and its matrix. IOP Conf Ser: Mater Sci Eng 2017;219:012030. https://doi.org/10.1088/1757-899x/219/1/012030.
[26] Nairn JA. On the use of shear-lag methods for analysis of stress transfer in unidirectional composites. Mech Mater 1997;26:63–80. https://doi.org/10.1016/S0167-6636(97)00023-9.
[27] Zhandarov S, Mäder E, Scheffler C, Kalinka G, Poitzsch C, Fliescher S. Investigation of interfacial strength parameters in polymer matrix composites: Compatibility and reproducibility. Adv Ind Eng Polym Res 2018;1:82–92. https://doi.org/10.1016/j.aiepr.2018.06.002.
[28] Zhandarov S, Mäder E. Determining the interfacial toughness from force–displacement curves in the pull-out and microbond tests using the alternative method. Int J Adhes Adhes 2016;65:11–8. https://doi.org/10.1016/j.ijadhadh.2015.10.020.
[29] Hou Y, Sun T. An improved method to make the microdroplet single fiber composite specimen for determining the interfacial shear strength. J Mater Sci 2012;47:4775–8. https://doi.org/10.1007/s10853-012-6317-2.